

# The Montreal Protocol avoided a reduction in the terrestrial carbon sink

Paul J. Young<sup>1,2,3\*</sup>, Anna B. Harper<sup>4,5</sup>, Chris Huntingford<sup>6</sup>, Nigel D. Paul<sup>1,7</sup>, Olaf Morgenstern<sup>8</sup>, Paul A. Newman<sup>9</sup>, Luke D. Oman<sup>9</sup>, Sasha Madronich<sup>10</sup> and Rolando R. Garcia<sup>10</sup>

<sup>1</sup> Lancaster Environment Centre, Lancaster University, Lancaster, UK

<sup>2</sup> Institute for Social Futures, Lancaster University, Lancaster, UK

<sup>3</sup> Centre of Excellence for Environmental Data Science, a joint centre of Lancaster University and the UK Centre of Ecology and Hydrology, UK

<sup>4</sup> College of Engineering, Mathematics, and Physical Sciences, University of Exeter, Exeter, UK

<sup>5</sup> Global Systems Institute, University of Exeter, Exeter, UK

<sup>6</sup> UK Centre for Ecology & Hydrology, Wallingford, UK

<sup>7</sup> Centre for Global Eco-Innovation, Lancaster University, Lancaster, UK

<sup>8</sup> National Institute of Water and Atmospheric Research, Wellington, Aotearoa New Zealand

<sup>9</sup> NASA Goddard Space Flight Center, Greenbelt, MD, USA

<sup>10</sup> National Center for Atmospheric Research, Boulder, CO, USA

\* paul.j.young@lancaster.ac.uk

**The control of ozone depleting substances (ODSs) through the Montreal Protocol means that the stratospheric ozone layer is now recovering<sup>1</sup>, avoiding increases in harmful surface ultraviolet (UV) radiation<sup>2,3</sup> and with co-benefits for climate change mitigation, since the controlled ODSs are potent greenhouse gases<sup>4-7</sup>. Here we use a modelling framework that couples ozone depletion, climate change, plant UV damage and the carbon cycle to explore how avoided UV increases and climate changes may have had benefits for the terrestrial biosphere and its capacity as a carbon sink. We explore a range of strengths for the impact of UV on plant growth consistent with published meta-analyses<sup>8-12</sup>, with a key assumption that they extend to the high UV levels in a world without the Montreal Protocol. Our central estimate is that there could have been 580 Gt (range 325–690 Gt) less carbon held in plants and soils by the end of this century (2080–2099) in a world without the Montreal Protocol, compared to the same climate projection but with ODS controls. We estimate that this change could have resulted in an additional 190 ppm (range 115–235 ppm) of atmospheric CO<sub>2</sub>, which may have led to 0.85 K (range 0.50–1.0 K) additional global mean surface temperature warming. Our findings suggest that the Montreal Protocol may also have helped to mitigate climate change through avoided decreases in the land carbon sink.**

The stratospheric ozone layer absorbs harmful, high energy ultraviolet light (UV-B; wavelength of 280–315 nm) that would otherwise threaten human<sup>13</sup> and ecosystem<sup>14,15</sup> health. Synthetic

chlorofluorocarbons (CFCs) were first identified as a risk to the ozone layer in 1974 by Molina and Rowland<sup>16</sup>, who showed that they could be a source of ozone-destroying chlorine atoms in the stratosphere. In the 1980s, CFC-derived chlorine was shown to be responsible for the severe ozone depletion over Antarctica during austral spring<sup>17</sup> (the “ozone hole”) and a greater understanding of the CFC threat to the whole ozone layer emerged<sup>1,18</sup>. In recognition of the ozone layer’s importance and the CFC threat, the Montreal Protocol was signed in 1987 to limit CFC production. Subsequent amendments completely phased-out CFC production along with several other halogenated ozone depleting substances (ODSs). As a result, atmospheric chlorine levels are decreasing and the ozone layer is recovering<sup>1</sup>. Moreover, since the controlled ODSs are also potent greenhouse gases<sup>4</sup>, the Montreal Protocol has also lessened radiative forcing and protected climate<sup>19</sup>.

The benefits of the Montreal Protocol have been explored through so-called “world avoided” experiments, using chemistry-climate models (CCMs) to simulate counterfactual scenarios where halogenated ODSs were never controlled<sup>20</sup>. Such studies have demonstrated significant avoided negative impacts for the ozone layer<sup>5–7</sup>, climate change<sup>7,19,21–23</sup>, surface UV-B<sup>3,24,25</sup> and human health<sup>2</sup>. No such world-avoided experiments have been conducted for terrestrial plants, crops or vegetation, although the impacts of UV-B on plant growth and development have been studied extensively (see ref. 14 for a summary). While the deleterious effects of UV-B are not thought to be concerning for current and projected UV-B levels<sup>11,14,26,27</sup>, the collected evidence from experimental data<sup>8</sup> would imply a substantial negative impact on above ground plant biomass from uncontrolled ozone depletion (and therefore high UV-B) as simulated for the world avoided. This would perturb the efficacy of the terrestrial land sink for atmospheric carbon dioxide (CO<sub>2</sub>), over and above any impact from ODS-driven climate change due to their properties as greenhouse gases. Such an interaction raises the possibility of hitherto unexplored links between the Montreal Protocol, the carbon cycle and CO<sub>2</sub>-driven climate change.

Here, we simulate the global impact of this interaction using a novel modelling framework, which combines meteorological and ozone (and then UV-B) output from the NIWA-UKCA CCM<sup>28</sup>; a weather generator; the land surface model JULES<sup>29,30</sup>, modified to include the impact of UV on the terrestrial biosphere; and an offline global carbon cycle and thermal model (see Methods). We use this framework to explore three scenarios. The world projected (worldProj) follows historical conditions to present day and then greenhouse gas and CFC emissions from the representative concentration pathway (RCP) 6.0<sup>31</sup> through the 21st century, including the mitigating impact of the Montreal Protocol on CFCs<sup>28</sup>. The second scenario is identical to worldProj, but with concentrations of CFCs fixed at their 1960 level (Fixed 1960 CFC). Finally, the world avoided (worldAvd) is identical to worldProj except that the trajectory of ODSs follows a scenario where a 3% per year growth of CFCs is prescribed<sup>19</sup>. Whilst this is clearly an extreme example of uncontrolled ozone depletion, it is consistent with other world avoided

studies<sup>6,7,21–23</sup> acting as a putative ‘worst case’ and providing a baseline against which other scenarios might be compared.

## The World Avoided environment

The ozone and climate conditions for worldAvd-like simulations have been reported before<sup>5–7,19,21–23,25</sup> so we only briefly discuss these aspects of our simulations. Whereas the ozone layer is projected to recover this century<sup>1</sup>, the continued increase in CFCs throughout the 21st century under the worldAvd scenario results in a large ozone depletion (Fig. 1a). In our simulations, the worldAvd ozone column departs from the recovery trajectory of the worldProj around the year 2000, with depletion accelerating until the 2040s when the CFC-driven chemistry leads to a worldwide ozone layer collapse<sup>7</sup>. By 2100, the global mean total column ozone drops to 90 Dobson units (DU), compared to 325 DU for the worldProj (~72% depletion). This trajectory is repeated for different latitude bands, but the proportionate loss is greater at higher latitudes. For instance, there is 78% less ozone in the northern mid-latitudes (30°–60°N) by 2100 for the worldAvd and 60% less ozone by 2100 for tropics (30°S/N). Yet, at only 115 DU the 2100 tropical ozone column is less than that ever observed for the Antarctic ozone hole<sup>1</sup>, and over a region whose savannahs and humid forests are responsible for 63% of the global net primary productivity<sup>32</sup> (NPP; the difference between the large opposing carbon fluxes from photosynthesis and ecosystem respiration).

In all our CCM simulations, concentrations of the greenhouse gases CO<sub>2</sub>, methane and nitrous oxide increase to ~2075, followed by a decrease in methane and a deceleration of the CO<sub>2</sub> increase<sup>31</sup>. This drives the monotonic increase in global mean air (1.5 m) temperature seen in all the simulations (Fig 1b). However, with a 2081–2100 mean warming of 3.2 K above the 1986–2005 mean (3.3 K above 1976–2005), the worldProj simulation warms more than the 1.4–3.1 K (5–95%) range reported for RCP6.0 in the fifth assessment report of the Intergovernmental Panel on Climate Change<sup>33</sup>. Along with their impact on ozone, the 3% per year increase in CFCs drives additional global mean air temperature warming in the worldAvd, resulting in a 2081–2100 change of 5.1 K. Therefore, even without any impact of the increased UV, we can surmise that the additional global warming under the worldAvd would have impacted the terrestrial biosphere and carbon cycle<sup>34,35</sup>.

What is the UV environment for terrestrial vegetation in the different simulations? To answer this, we accounted for the sensitivity of terrestrial plants to particular UV wavelengths through the use of the generalised plant action spectrum<sup>36,37</sup> in order to show the change in clear sky, biologically active UV fluxes (UV<sub>plant</sub>) that result from ozone changes (Fig. 1c). Mirroring the total ozone column (Fig. 1a), global annual mean UV<sub>plant</sub> for the worldAvd clearly separates from the worldProj and Fixed 1960 CFC trajectories after 2000, doubling compared to the 1976–2005 baseline by ~2050 and exceeding that baseline by a factor of 4.5 by the end of century. Similar timings and magnitudes of change are evident in different regions. Moreover, absolute UV<sub>plant</sub>

fluxes in both the northern (30°–60° N) and southern (30°–60° S) mid-latitudes exceed the present day tropical values by ~2050.

To translate the  $UV_{\text{plant}}$  into a response and impact on the terrestrial biosphere, we modified the rate of carbon assimilation in JULES. For our reference UV response strength, we applied a 3% reduction in assimilation for a 10% increase in  $UV_{\text{plant}}$ , which translates to a reduction in NPP. This dose-response is derived from an analysis conducted by the Environmental Effects Assessment Panel of the Montreal Protocol<sup>8</sup> and is broadly consistent with the magnitude of biomass responses across species in other meta-analyses<sup>9–12</sup> (see Methods and Extended Data Table 2). Our calculations account for simulated clouds, which are, conservatively<sup>38</sup>, assumed to be opaque to UV. Furthermore, we assume that vegetation is acclimated to local UV conditions at particular times of year and we only apply a carbon assimilation impact when  $UV_{\text{plant}}$  exceeds its local climatology (1976–2005 average from Fixed 1960 CFCs) plus its temporal standard deviation. Even after accounting for clouds and local acclimatisation, carbon assimilation in the worldAvd simulation is decreased by 20–40% by the 2030s and by 70–90% by the 2050s for northern mid-latitudes, and by 60–80% by the 2090s over the tropical forests (Fig. 1d). Seasonality of the scaling is important for the highly vegetated northern mid-latitudes: by the mid-2040s, the ozone depletion-driven early spring UV increases extend into summer, with a >80% downward scaling of carbon assimilation occurring throughout the entire growing season north of 40°N.

## **World Avoided carbon cycle changes**

Our modelling framework accounts for the spatial distributions of vegetation and changes in climate and  $UV_{\text{plant}}$  allowing us to calculate globally-integrated impacts on NPP and the resultant effects on carbon cycling in the terrestrial biosphere (Fig. 2). We test the sensitivity of our results to uncertainty in the strength of the UV-plant dose-response through additional replicates for each scenario, with the UV response strength scaled to be 10%, 50% and 150% the reference magnitude: i.e., respectively a 0.3%, 1.5% and 4.5% reduction in NPP for a 10% increase in  $UV_{\text{plant}}$ . UV damage on the biosphere within a given scenario is quantified by comparing the simulations against an additional replicate, where there is no UV effect on NPP (i.e., a UV response strength of 0). In addition to the direct effect of UV on NPP, there is a feedback effect from vegetation change: an increased UV initially lowers NPP, which reduces leaf area and photosynthetic capacity, which in turn results in lower NPP.

The UV impact is apparent from the beginning of the simulations for both worldAvd and worldProj (inset Fig. 2b). For the worldProj, UV damage on NPP peaks in the late 1990s, consistent with the peak in ozone depletion. Here, UV increases reduce total land carbon (C) accumulation by approximately 0.5 Gt C / yr in the 1990s, ranging from 0.3–0.9 Gt C / yr for the 50 and 150% UV response strengths (inset Fig. 2d). As the ozone layer recovers, so does the terrestrial biosphere, with most of the initial damage and subsequent recovery occurring in the

northern mid-latitudes (30°N–60°N; Extended Data Fig. 1a). NPP in the worldProj continues to increase until the end of the simulation, finishing ~30% higher than its 1980 values (Fig. 2a), driven by increasing atmospheric CO<sub>2</sub> concentrations (CO<sub>2</sub>-fertilisation) and modulated by temperature changes<sup>39</sup>.

In the worldAvd, the UV-induced reduction to global NPP accelerates during the 2040s (Fig 2a), and is approximately 50 Gt C / yr by 2100 (Fig. 2b). From the 2040s to the 2050s, global NPP decreases by 14 Gt C / yr, with about half of this decrease occurring in the northern mid-latitudes (Extended Data Fig. 1a), where large increases in UV coincide with productive agricultural and forest regions. An NPP decrease in the tropics (30°N/S; Extended Data Fig. 1b) becomes more apparent from 2050 onwards when UV<sub>plant</sub> exceeds the climatology, although this is delayed for the reduced (50%) UV response strength simulation and advanced for the increased (150%) UV response strength simulation. Tropical NPP decreases from 38 Gt C / yr for 1976–2005 to 30 Gt C / yr by the 2050s (15–34 Gt C / yr, for the 50% and 150% UV response strengths) and 19 Gt C / yr (8–32 Gt C / yr) for the 2060s.

By the end of the century (2080–2099), global NPP in worldAvd is only 12 Gt C / yr (3–24 Gt C / yr) compared to 77 Gt C / yr in the worldProj (Fig. 2a). As a result of these large reductions in net carbon uptake, global terrestrial biomass decreases from 340 Gt C (1976–2005) to 245 Gt C (200–285 Gt C) by the end of the century (not shown). In our simulations, vegetation fractions are held fixed, so large-scale biome shifts do not occur. However, the less productive biosphere turns over less carbon into soils, and large losses of soil carbon follow the declines in NPP. Overall, by the end of the century the land (vegetation plus soil) loses 535 Gt C in the worldAvd scenario (415–645 Gt C), compared to a gain of 45 Gt C in the worldProj scenario; i.e., there is 580 Gt less carbon stored in the land for the worldAvd versus the worldProj (Fig 2c).

Even with a substantially weakened (10%) UV response strength, NPP is 35 Gt C / yr by the end of the century, which is less than half of the worldProj value (Fig. 2a), resulting in a 325 Gt C reduction in the terrestrial carbon stores over the century (Fig. 2c). The weakened effect delays the onset of changes to the carbon cycle, and the impacts on NPP and the terrestrial carbon stores becomes apparent 15–20 years later than the other worldAvd simulations. However, after ~2045 dramatic impacts can be seen in the northern hemisphere: for 60°N–85°N, NPP drops from 3.7 Gt C / yr to 0.06 Gt C / yr between 2048–2054 and never recovers. In comparison, tropical impacts are delayed until the 2080s and are relatively smaller (NPP decreases from 38 Gt C / yr for 1976–2005 to 32 Gt C / yr for 2080–2099) due to smaller relative changes in UV<sub>plant</sub> levels compared to higher latitudes (Fig 1d). With the UV effect set to zero, we can still see an impact of uncontrolled CFC emissions on the carbon cycle. By itself, the warmer climate of the worldAvd shifts the balance between primary productivity and ecosystem respiration more towards the latter, reducing end-century NPP by 6 Gt C / yr (Fig. 2a) and the terrestrial carbon stores by 50 Gt C (Fig. 2c) compared to the worldProj.

We used our framework to translate the changes in terrestrial carbon stores to an impact on atmospheric CO<sub>2</sub> levels (Fig. 3a), accounting for the feedback between the land, ocean and atmospheric stores of the carbon cycle, including CO<sub>2</sub> fertilisation (see Methods). By 2040, the UV-induced reduction in terrestrial carbon stores for the worldAvd sets the atmospheric CO<sub>2</sub> concentrations on a new, higher trajectory than the base RCP6.0 scenario. At 2060, worldAvd CO<sub>2</sub> levels are close to 600 ppm (570–625 ppm for 50% and 150% UV response strengths), which is 85 ppm (55–110 ppm) or 16% (11–21%) higher than the worldProj case. By the end of the century (2080–2099), CO<sub>2</sub> levels are 827 ppm (781–872 ppm) for the worldAvd, compared to 636 ppm for the worldProj, or 30% (23–37%) higher.

Higher atmospheric CO<sub>2</sub> concentrations result in increased radiative forcing and a higher global mean air temperature (Fig. 3b). Overall, at the end of the century, the worldAvd warms an additional 2.5 K (2.4–2.7 K) above the RCP6.0 baseline in the worldProj. Of this warming, 1.7 K comes from the previously explored<sup>19</sup> additional radiative forcing due to the higher CFCs in worldProj. Newly quantified here is the additional 0.85 K (0.65–1.0 K) global mean air temperature warming – half as much again – arising from the higher atmospheric CO<sub>2</sub> concentrations due to the damaging effect of UV on terrestrial carbon stores. We note that the UV impacts on the carbon cycle in the worldAvd are large enough that the magnitude of the atmospheric CO<sub>2</sub> concentration and temperature changes are not very sensitive to the underlying CO<sub>2</sub> climate scenario (see Extended Data Table 1). We also note that the worldAvd global mean air temperature is marginally lower than for worldProj at the start of the simulations, which is due to the real-world CFCs increasing faster than the 3% per year in the worldAvd simulation.

The additional CO<sub>2</sub> and warming under the worldAvd is still apparent for the 10% UV response strength, with 115 ppm extra CO<sub>2</sub> above the worldProj by the end of the century, resulting in 0.50 K of additional warming above that due to the CFCs. This result may appear surprising, as a plant response to increased UV radiation of this smaller magnitude is unlikely to be detectable as a significant change in experimental studies<sup>11</sup>. However, as evident from the NPP and carbon store decreases (Fig. 2), the small short-term impacts are compounded over decades by the large increases in UV radiation in the worldAvd.

As with many efforts to aggregate small-scale processes to large-scale ecology-climate interactions, we are limited by a relative paucity of data for some aspects. For our modelling, a particular source of uncertainty is the still limited understanding of plant UV dose responses at the very high UV doses in the worldAvd simulation and remaining questions around plant action spectra (see Methods). We also recognise the lack of data on field UV responses that cover the world's ecosystems and how plants and ecosystems might adapt to the extreme UV environments that would occur with uncontrolled ozone depletion. Moreover, with the development of high quality NPP dataset and a sophisticated detection and attribution algorithm,

future work might be able to constrain the UV-carbon cycle impact over the observed ozone depletion and recovery. There are uncertainties in other elements of our modelling, including the lack of full coupling between the CCM and land surface model and exclusion of other UV-biosphere interactions, such as additional CO<sub>2</sub> from enhanced photodegradation and irradiation of organic matter<sup>40</sup>. On the other hand, higher UV levels would decrease the methane chemical lifetime – and therefore its concentrations – due to enhanced hydroxyl radical levels.

Nevertheless, given our conservative assumptions and the simulated response with even our weakest UV response strength, we are confident that our experiment and framework presents a defensible, order-of-magnitude estimate of the impact of the Montreal Protocol on the ozone-UV-biosphere-carbon cycle-climate system. That impact is a substantial climate system co-benefit of the Montreal Protocol, whereby the avoided damage to the ozone layer prevents UV damage to vegetation, which in turn allows larger terrestrial carbon stores to exist. This acts in addition to well-established climate-protection achieved by controlling ODSs that are potent greenhouse gases<sup>19</sup>.

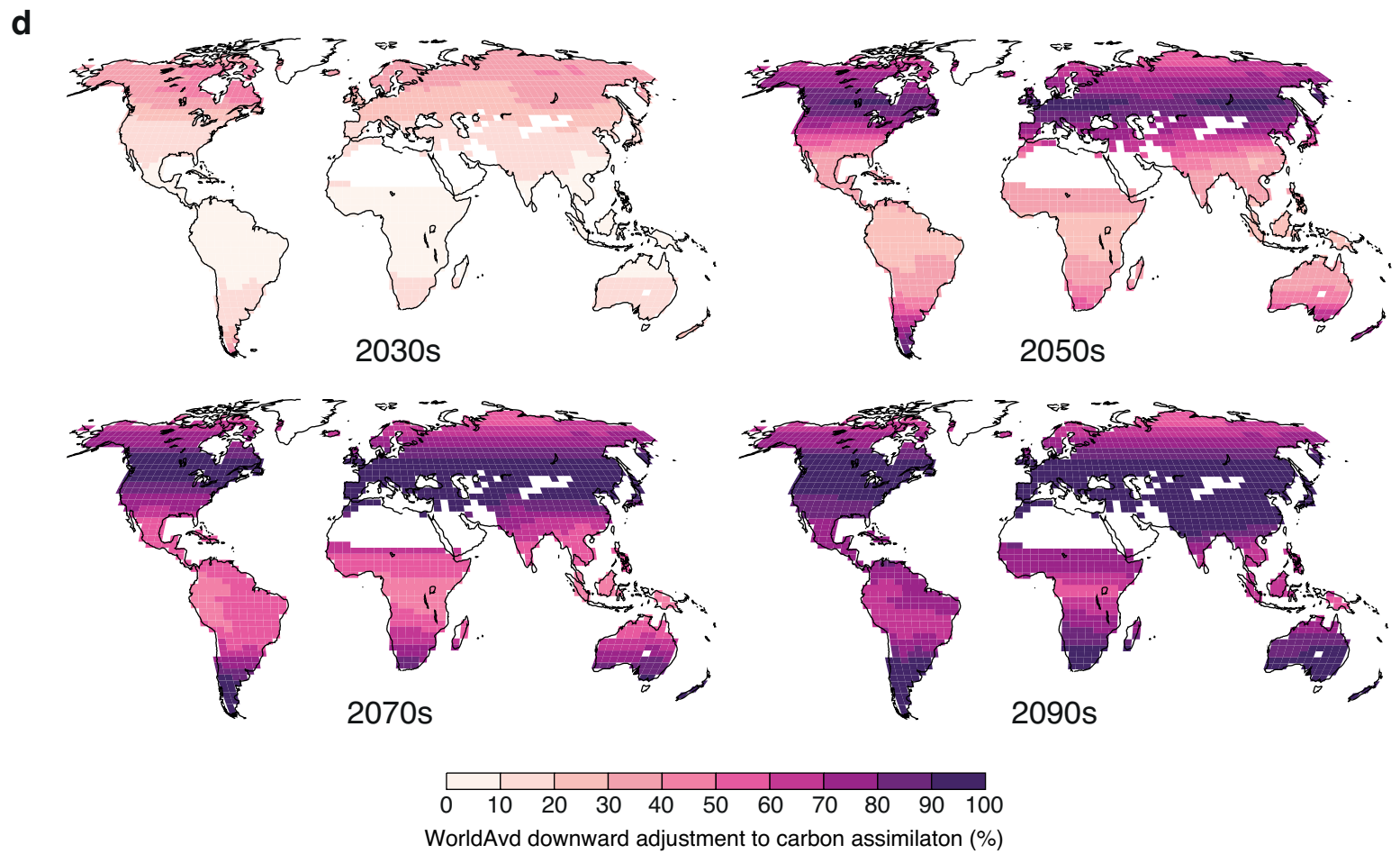
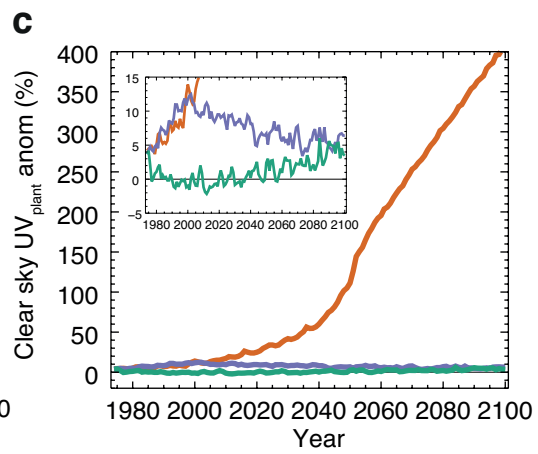
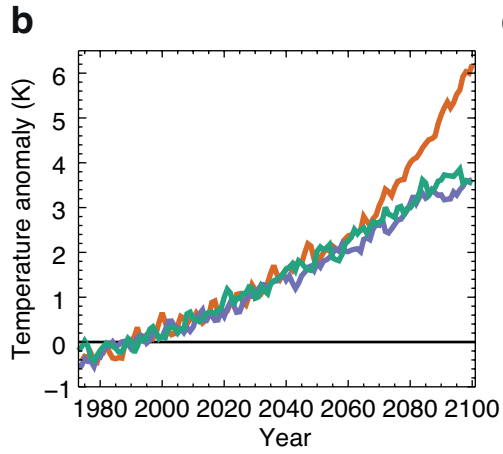
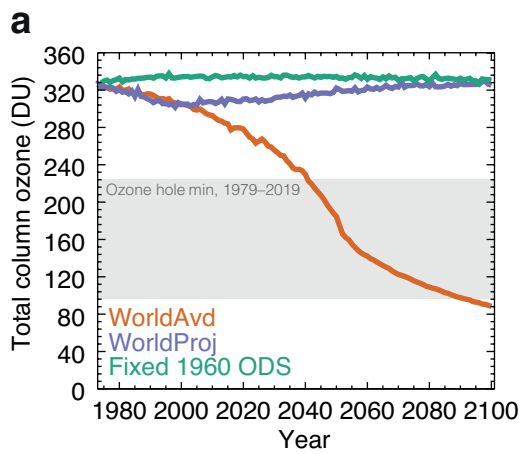
We have demonstrated global benefits by quantifying an explicit connection of the Montreal Protocol with the carbon cycle and thus CO<sub>2</sub>-driven climate change. Many of the effects on global carbon cycling in the world have only become evident from the 2040s and it is intriguing to speculate at what point such effects in a world without the Montreal Protocol would have prompted ozone protection. The damage reported here to terrestrial vegetation, and by inference the damage to crop plants, would likely have triggered action to prevent our extreme “world avoided” scenario, and it is unlikely our 2100 projections would have occurred as simulated even without the 1987 Montreal Protocol. Extensions to this work could exploit our modelling framework to explore more nuanced “Montreal delayed” projections as well as scenarios more consistent with our current trajectory. These should recognise the real-world ozone layer threats from unauthorised CFC emissions<sup>41</sup> and stratospheric geoengineering<sup>42</sup>, but also the possibility of myriad, more complex UV-biosphere interactions that would be relevant at the lower UV levels expected with ozone layer recovery<sup>40</sup>. Overall, using ozone depletion to explore the impacts of delay or dilution of a global policy response to a global environmental challenge may have relevance well beyond the Montreal Protocol.

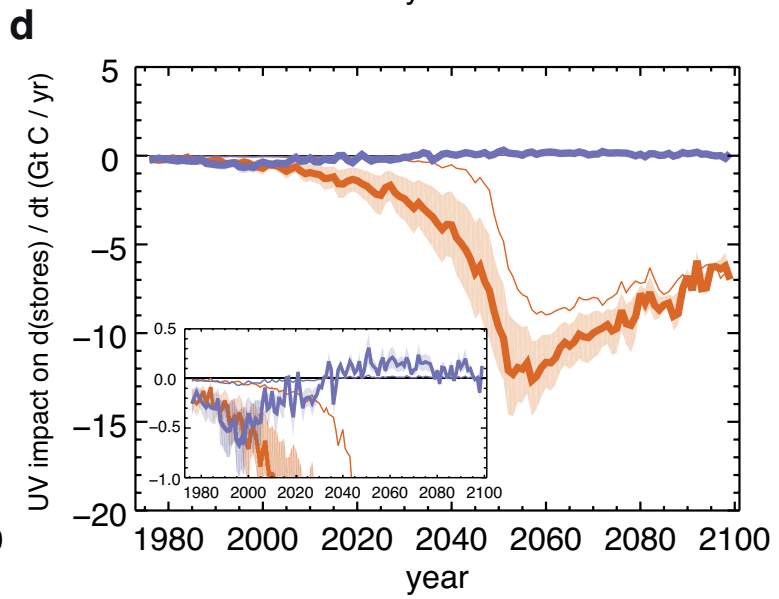
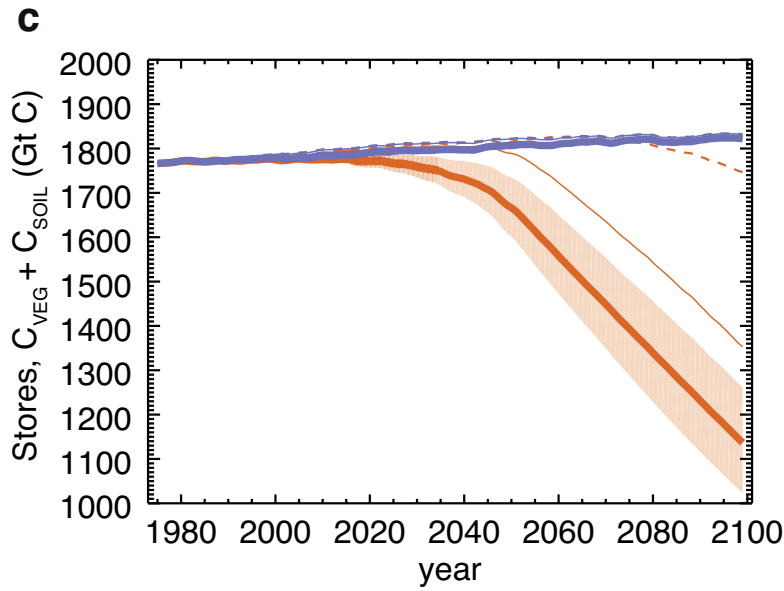
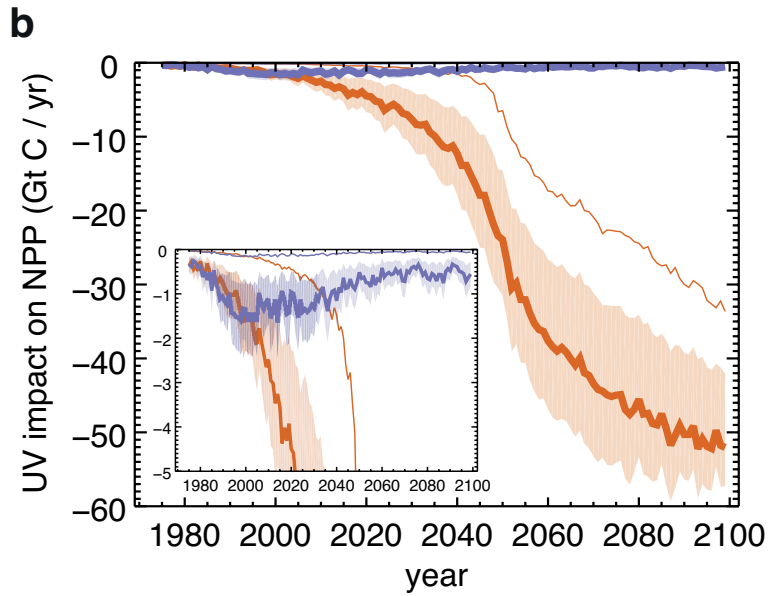
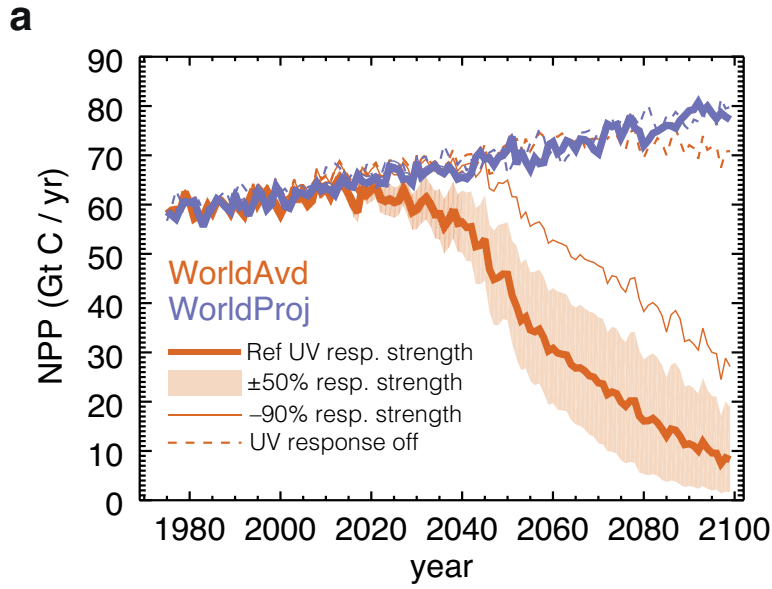
## References

1. WMO (World Meteorological Organization). *Scientific Assessment of Ozone Depletion: 2018*. Global Ozone and Research Monitoring Project–Report No. 58, Geneva, Switzerland (2018).
2. van Dijk, A. *et al.* Skin cancer risks avoided by the Montreal Protocol—Worldwide modeling integrating coupled climate-chemistry models with a risk model for UV. *Photochem. Photobiol.* **89**, 234–246 (2013).
3. McKenzie, R. *et al.* Success of Montreal Protocol demonstrated by comparing high-quality UV measurements with ‘World Avoided’ calculations from two chemistry-climate models. *Sci. Rep.* **9**, 1–13 (2019).
4. Ramanathan, V. Greenhouse effect due to chlorofluorocarbons: Climatic implications. *Science* **190**, 50–52 (1975).
5. Morgenstern, O. *et al.* The world avoided by the Montreal Protocol. *Geophys. Res. Lett.* **35**, L16811 (2008).
6. Newman, P. A. *et al.* What would have happened to the ozone layer if chlorofluorocarbons (CFCs) had not been regulated? *Atmos. Chem. Phys.* **9**, 2113–2128 (2009).
7. Garcia, R. R., Kinnison, D. E. & Marsh, D. R. ‘World avoided’ simulations with the Whole Atmosphere Community Climate Model. *J. Geophys. Res.* **117**, D23303 (2012).
8. Ballaré, C. L., Caldwell, M. M., Flint, S. D., Robinson, S. A. & Bornman, J. F. Effects of solar ultraviolet radiation on terrestrial ecosystems. Patterns, mechanisms, and interactions with climate change. *Photochem. Photobiol. Sci.* **10**, 226–241 (2011).
9. Newsham, K. K. & Robinson, S. A. Responses of plants in polar regions to UVB exposure: a meta-analysis. *Glob. Chang. Biol.* **15**, 2574–2589 (2009).
10. Li, F.-R., Peng, S.-L., Chen, B.-M. & Hou, Y.-P. A meta-analysis of the responses of woody and herbaceous plants to elevated ultraviolet-B radiation. *Acta Oecol.* **36**, 1–9 (2010).
11. Searles, P. S., Flint, S. D. & Caldwell, M. M. A meta-analysis of plant field studies simulating stratospheric ozone depletion. *Oecologia* **127**, 1–10 (2001).
12. Fu, G. & Shen, Z.-X. Effects of enhanced UV-B radiation on plant physiology and growth on the Tibetan Plateau: a meta-analysis. *Acta Physiol. Plant* **39**, 85 (2017).
13. Lucas, R. M. *et al.* Human health in relation to exposure to solar ultraviolet radiation under changing stratospheric ozone and climate. *Photochem. Photobiol. Sci.* **18**, 641–680 (2019).
14. Bornman, J. F. *et al.* Linkages between stratospheric ozone, UV radiation and climate change and their implications for terrestrial ecosystems. *Photochem. Photobiol. Sci.* **18**, 681–716 (2019).
15. Williamson, C. E. *et al.* The interactive effects of stratospheric ozone depletion, UV radiation, and climate change on aquatic ecosystems. *Photochem. Photobiol. Sci.* **18**, 717–746 (2019).
16. Molina, M. J. & Rowland, F. S. Stratospheric sink for chlorofluoromethanes: chlorine atom-catalysed destruction of ozone. *Nature* **249**, 810–812 (1974).
17. Solomon, S., Garcia, R. R., Rowland, F. S. & Wuebbles, D. J. On the depletion of Antarctic ozone. *Nature* **321**, 755–758 (1986).
18. Solomon, S. Stratospheric ozone depletion: A review of concepts and history. *Rev.*

- Geophys.* **37**, 275–316 (1999).
19. Velders, G. J. M., Andersen, S. O., Daniel, J. S., Fahey, D. W. & McFarland, M. The importance of the Montreal Protocol in protecting climate. *Proc. Natl. Acad. Sci. U. S. A.* **104**, 4814–4819 (2007).
  20. Prather, M., Midgley, P., Rowland, F. S. & Stolarski, R. The ozone layer: the road not taken. *Nature* **381**, 551–554 (1996).
  21. Wu, Y., Polvani, L. M. & Seager, R. The importance of the Montreal Protocol in protecting Earth’s hydroclimate. *J. Clim.* **26**, 4049–4068 (2013).
  22. Polvani, L. M., Camargo, S. J. & Garcia, R. R. The importance of the Montreal Protocol in mitigating the potential intensity of tropical cyclones. *J. Clim.* **29**, 2275–2289 (2016).
  23. Previdi, M. & Polvani, L. M. Impact of the Montreal Protocol on Antarctic surface mass balance and implications for global sea level rise. *J. Clim.* **30**, 7247–7253 (2017).
  24. Chipperfield, M. P. *et al.* Quantifying the ozone and ultraviolet benefits already achieved by the Montreal Protocol. *Nat. Commun.* **6**, 7233 (2015).
  25. Newman, P. A. & McKenzie, R. UV impacts avoided by the Montreal Protocol. *Photochem. Photobiol. Sci.* **10**, 1152–1160 (2011).
  26. Neugart, S. & Schreiner, M. UVB and UVA as eustressors in horticultural and agricultural crops. *Sci. Hortic.* **234**, 370–381 (2018).
  27. Fiscus, E. L. & Booker, F. L. Is increased UV-B a threat to crop photosynthesis and productivity? *Photosynth. Res.* **43**, 81–92 (1995).
  28. Morgenstern, O. *et al.* Review of the global models used within phase 1 of the Chemistry–Climate Model Initiative (CCMI). *Geoscientific Model Development* **10**, 639–671 (2017).
  29. Best, M. J. *et al.* The Joint UK Land Environment Simulator (JULES), model description–Part 1: energy and water fluxes. *Geoscientific Model Development* **4**, 677–699 (2011).
  30. Clark, D. B. *et al.* The Joint UK Land Environment Simulator (JULES), model description–Part 2: carbon fluxes and vegetation dynamics. *Geoscientific Model Development* **4**, 701–722 (2011).
  31. van Vuuren, D. P. *et al.* The representative concentration pathways: an overview. *Clim. Change* **109**, 5–31 (2011).
  32. Barlow, J. *et al.* The future of hyperdiverse tropical ecosystems. *Nature* **559**, 517–526 (2018).
  33. Collins, M. *et al.* Long-term climate change: projections, commitments and irreversibility. in *Climate Change 2013-The Physical Science Basis: Contribution of Working Group I to the Fifth Assessment Report of the Intergovernmental Panel on Climate Change* 1029–1136 (Cambridge University Press, 2013).
  34. Cox, P. M., Betts, R. A., Jones, C. D., Spall, S. A. & Totterdell, I. J. Acceleration of global warming due to carbon-cycle feedbacks in a coupled climate model. *Nature* **408**, 184–187 (2000).
  35. Heimann, M. & Reichstein, M. Terrestrial ecosystem carbon dynamics and climate feedbacks. *Nature* **451**, 289–292 (2008).
  36. Caldwell, M. M. Solar UV irradiation and the growth and development of higher plants. in *Photophysiology, Current Topics in Photobiology and Photochemistry* (ed. Giese, A. C.) vol. VI 131–177 (Academic Press, 1971).
  37. Caldwell, M. M., Camp, L. B., Warner, C. W. & Flint, S. D. Action spectra and their

- key role in assessing biological consequences of solar UV-B radiation change. in *Stratospheric Ozone Reduction, Solar Ultraviolet Radiation and Plant Life* (eds. Worrest, R. C. & Caldwell, M. M.) vol. 8 87–111 (Springer, 1986).
38. Calbó, J., Pagès, D. & González, J. Empirical studies of cloud effects on UV radiation: A review. *Rev. Geophys.* **43**, 5199 (2005).
  39. Arora, V. K. *et al.* Carbon–concentration and carbon–climate feedbacks in CMIP5 Earth system models. *J. Clim.* **26**, 5289–5314 (2013).
  40. Williamson, C. E. *et al.* Solar ultraviolet radiation in a changing climate. *Nat. Clim. Chang.* **4**, 434–441 (2014).
  41. Rigby, M. *et al.* Increase in CFC-11 emissions from eastern China based on atmospheric observations. *Nature* **569**, 546–550 (2019).
  42. Tilmes, S., Garcia, R. R., Kinnison, D. E., Gettelman, A. & Rasch, P. J. Impact of geoengineered aerosols on the troposphere and stratosphere. *J. Geophys. Res.* **114**, D12305 (2009).
  43. NASA. NASA Ozone Watch website. [https://ozonewatch.gsfc.nasa.gov/meteorology/annual\\_data.html](https://ozonewatch.gsfc.nasa.gov/meteorology/annual_data.html) (2019).





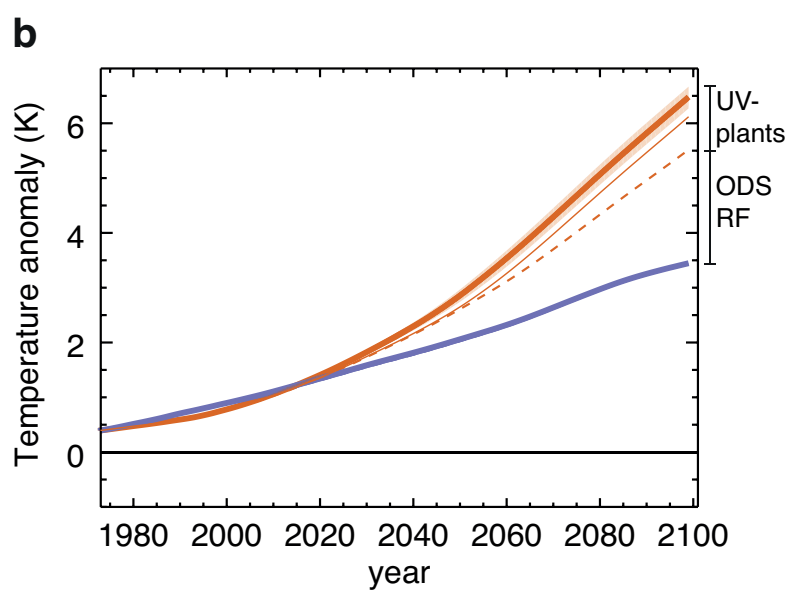
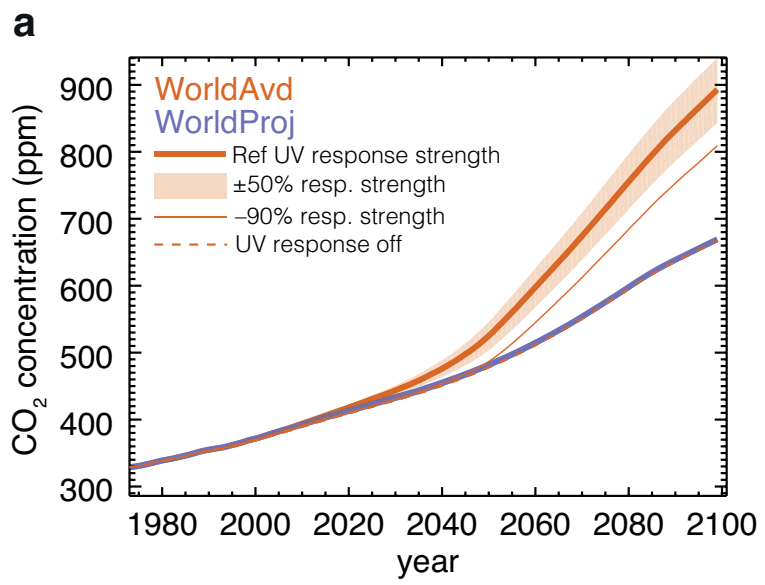


## Figure captions

**Figure 1 | The ozone, climate and biologically-active UV of different futures.** **a, b,** Time series of **(a)** the global mean total column ozone (Dobson Units, DU) alongside the range of the minimum of Southern Hemisphere mean total column ozone for 21 September–16 October over 1979–2019 (grey shading)<sup>43</sup> and **(b)** the global mean air temperature (Kelvin, K), as an anomaly to the 1976–2005 average for the “world projected” (worldProj, green; RCP6.0), “world avoided” (worldAvd, blue; RCP6.0 but with 3% per year increases of chlorofluorocarbons (CFCs) from 1974<sup>19</sup>), and “Fixed 1960 CFCs” (orange-brown; RCP6.0, but CFCs fixed at their 1960 level) simulations, all from the NIWA-UKCA chemistry climate model<sup>28</sup> output. **c,** Global mean clear sky, generalised plant action spectrum-weighted<sup>36</sup> UV surface fluxes ( $UV_{\text{plant}}$ ) for the same three simulations as **(a)** and **(b)** expressed as a percentage change relative to the 1976–2005 average in the Fixed 1960 CFCs simulation, with a reduced y-axis inset panel to highlight the UV changes in the WorldProj simulation. **d,** Maps of the year-round, decadal average scale factor applied to net primary productivity (NPP) for the worldAvd simulation, after accounting for clouds, as applied in the JULES land surface model<sup>29,30</sup>. Grid squares with a vegetation fraction less than 10% are masked white.

**Figure 2 | Impacts for the terrestrial carbon cycle productivity and stores.** **a, b,** Time series of **(a)** net primary productivity (NPP) and **(b)** the direct impact of UV on NPP, as determined from the reference UV response strength (3% NPP reduction for 10% increase in weighted UV), for the worldProj (blue) and worldAvd (orange) simulations (as per Fig. 1), all output from the JULES land surface model<sup>29,30</sup> and in units of gigatonnes of carbon per year (Gt C / yr). **c, d,** Time series from the same set of simulations showing **(c)** the terrestrial carbon stores (vegetation,  $C_{\text{VEG}}$ , plus soils,  $C_{\text{SOIL}}$ ) in units of gigatonnes of carbon (Gt C), and **(d)** the impact of UV on the rate of carbon accumulation in the terrestrial carbon stores, which is determined by subtracting rates from the “UV damage on” simulations from “UV damage off” simulations (i.e., just the impact of climate changes), in units of Gt C / yr. The dashed orange lines in **(a)** and **(c)** are results from the “UV damage off” simulations, the thin orange line shows the impact of reducing the UV response strength by 90%, and the shading about the thick orange lines indicates the range of the responses from increasing and decreasing UV response strength by 50% with respect to the reference UV case. The inset in panels in **(b)** and **(d)** highlight the UV damage apparent in the worldProj scenario, and have reduced y-axes compared to their main plot.

**Figure 3 | The impact UV-driven vegetation changes on atmospheric CO<sub>2</sub> and surface temperature.** Time series of **(a)** atmospheric CO<sub>2</sub> concentrations and **(b)** global mean air temperature anomalies for the worldProj (blue) and worldAvd (orange), estimated using a carbon cycle model with the land surface model (JULES) output.

## METHODS

To investigate the system of ozone, UV, carbon cycle and climate impacts, we developed a novel modelling framework that couples output from a chemistry climate model (CCM), to a terrestrial biosphere model, to global box models of energy balance and the carbon cycle, involving some additional calculations in between. The components of this modelling framework are described below.

### NIWA-UKCA CCM

Simulations to generate climate and ozone temperature data were completed using the National Institute for Water and Atmospheric (NIWA) research version of the UK Chemistry and Aerosol (UKCA) global CCM<sup>28,44</sup>, which sits within the general circulation model framework of HadGEM3<sup>45</sup>. The atmospheric model resolution is  $3.75^\circ \times 2.5^\circ$  with 60 vertical levels, with a  $\sim 2^\circ$  horizontal resolution and 31 levels for the ocean. The chemistry scheme includes lumped treatments of the chlorine source gases as CFC-11 ( $\text{CCl}_3\text{F}$ ) and CFC-12 ( $\text{CCl}_2\text{F}_2$ ) and the bromine source gases as  $\text{CHBr}_3$ ,  $\text{CH}_2\text{Br}_2$  and  $\text{CHBr}_3$ . In line with the simulation protocols of the Chemistry Climate Model Initiative (CCMI)<sup>28</sup>, all three simulations here follow the historical and RCP6.0 scenarios for (non-halogenated) greenhouse gases. For CFCs, worldProj follows the A1 scenario of the World Meteorological Organization<sup>46</sup>, worldAvd follows the MR74 scenario of Ref. 19, and Fixed 1960 CFCs fixes their concentrations at their 1960 level.

Model performance for ozone is state-of-the-art<sup>5,28</sup> and the ozone sensitivity to external forcings (climate and ODSs) compares well to other models<sup>47</sup>. Additionally, the model radiation code<sup>48</sup> compares very favourably against comprehensive line-by-line models, especially for the response to changes in key gases, including ozone<sup>49</sup>. However, like many climate models, there are biases in cloud position and amount<sup>50</sup> which will impact our estimates of  $\text{UV}_{\text{plant}}$  fluxes.

### Weather generator

Monthly mean meteorological data from the CCM was disaggregated to a 3-hourly time resolution to use as input for the JULES land surface model (see below). This process used 1979–2017 output from ECMWF ERA-Interim reanalysis data<sup>51</sup> to generate estimates of high-frequency “weather” features, but which also reflect the longer-term climatic changes projected by the CCM. Time series were generated as a function of location for the following variables: (1) temperature, (2) zonal (u) wind, (3) meridional (v) wind, (4) downwelling longwave radiation, (5) humidity, (6) atmospheric pressure, (7) all sky downwelling shortwave (SW) radiation, (8) clear-sky downwelling SW radiation, (9) precipitation and (10) cloud cover. JULES requires all of these variables, except for the clear-sky downward shortwave radiation and cloud cover; however, these two quantities are needed in order to calculate the UV damage effect.

The humidity and pressure fields are relatively invariant within a month, and so these are kept as those of NIWA-UKCA, and hence fixed for each three-hour period. For variables (1)–(4), a

relatively simple temporal disaggregation method was employed, where, as a function of month and location, a random year's data was extracted from the reanalysis. The time series was then scaled such that the monthly mean of the disaggregated 3-hourly data was equal to the corresponding monthly mean from the CCM. Overall, this provides each location with a single time series, with mean changes that follow the CCM but with daily and sub-daily weather features based on the reanalysis, albeit lacking autocorrelation across monthly boundaries.

Particular attention was paid to the calculation of clear sky and all sky downwelling SW radiation and cloud cover, as these strongly influence the forcings from the UV-damage effect we incorporated into JULES. The starting point for this part of the weather generator was to create a high temporal resolution (sub-daily) estimate of clear-sky downwelling SW. Due to the lack of this variable in the reanalysis output, we used clear-sky photosynthetically active radiation, which gives the daily "shape" of clear-sky downwelling SW radiation, and which was then scaled to match the clear sky downwelling SW from the CCM output. The next step was to make a time series for all-sky downwelling SW. To achieve this, we implemented a form of Markov chain, based on the reanalysis data. Based on the value at the current timestep, this procedure associated probabilities with a range of values for the fraction of all-sky downwelling SW divided by clear-sky downwelling SW at the next timestep. Such extra complexity ensures that "memory" effects are reproduced; for example, if there is a substantial suppression of SW at one time step (i.e., extensive cloud cover), then there is a higher chance that such suppression will still be present at the next time step. For each location and month, a lookup table was produced containing probabilities linking ranges of this all-sky/clear-sky fraction between time steps. (Note, this table was based on *net* clear-sky and all-sky downwelling SW, as these are the only available ERA-Interim outputs.) Using a random number generator, these tables were used to create a synthetic 3-hourly time series of all sky downwelling SW, which was again normalised to match the monthly means from the CCM.

The calculation of high-frequency cloud cover and precipitation variability followed a similar procedure to that of downwelling SW. For each location and month, two tables of probabilities were constructed that link cloud cover and precipitation to the previous timestep's all-sky/clear-sky downwelling SW fraction. Again, we then used a random number generator to generate realistic estimates of cloud cover and precipitation that preserve the autocorrelation implicit within reanalysis. Finally, these last two time series are also normalised such that their monthly means match those of the CCM simulations.

### **Ozone to UV**

Plant-weighted<sup>36</sup> surface UV fluxes ( $UV_{\text{plant}}$ ) appropriate to the total column ozone from NIWA-UKCA were made using a relationship between total column ozone and  $UV_{\text{plant}}$  determined from previous, world avoided calculations using the Atmospheric Laboratory for Applications and Science 3 (ATLAS-3) extraterrestrial solar flux and the Total Ozone Mapping Spectrometer

radiative transfer code (TOMRAD) (See ref. 6 for a discussion of the implementation). The relationship used a 3rd-order polynomial fit between total column ozone and the natural logarithm of  $UV_{\text{plant}}$  as a function of month, latitude and longitude, capturing the effects of variations in top-of-atmosphere solar flux (month, latitude) as well as surface elevation (longitude). The resulting monthly mean, clear sky,  $UV_{\text{plant}}$  were linearly interpolated to a daily time axis. The percentage change between  $UV_{\text{plant}}$  and a reference value was calculated as a function of location and day of the year, with the reference values derived from the 1976–2005 climatology of the Fixed 1960 CFC simulation, using the mean plus temporal standard deviation. Overall, this creates the assumption that plants are adapted to their local UV conditions and a given time of year, and that – assuming a normal distribution – they would express some negative impact at UV levels experienced ~16% of the time under non-ozone depletion conditions.

### **UV to plant response**

The percentage change in  $UV_{\text{plant}}$  was converted to a clear sky UV scale factor, used to adjust carbon assimilation in the terrestrial model, JULES. Our reference point was to calculate this clear sky UV scale factor assuming a UV response strength of a 3% reduction in carbon assimilation for a 10% increase in  $UV_{\text{plant}}$ . We additionally conducted sensitivity tests using simulations that considered 1.5x, 0.5x and 0.1x the reference UV response strength. Together, the four UV response strengths in our simulations are based on the four published meta-analyses of plant responses to  $UV_{\text{plant}}$ <sup>9–12</sup>. Our aim was not to derive precise values of plant dose responses to  $UV_{\text{plant}}$  but to clarify the broad magnitude of generalised responses, both as context for our reference response strength and to inform our sensitivity analysis.

Our reference UV response strength of a 3% reduction in biomass for a 10% increase in  $UV_{\text{plant}}$  is derived from the analysis of the Environmental Effects Assessment Panel of the Montreal Protocol<sup>8</sup>, and ultimately from Newsham and Robinson<sup>9</sup>. While their data for above-ground biomass is limited to a 50% increase over ambient  $UV_{\text{plant}}$ , they also demonstrate a linear relationship for an impact on leaf area that extends to a 100% increase. That analysis is limited to high latitude species, but the other meta-analyses cover a much wider range of species and geographical origins, and report the response of a wider range of growth parameters (see Extended Data Table 2). The meta-analysis of 142 studies of Li et al.<sup>10</sup> divides plant responses to  $UV_{\text{plant}}$  into “low” (< 40%) and “high” (40–100%) increases over ambient. Fu and Shen<sup>12</sup> analysed data from 28 field supplementation experiments, with  $UV_{\text{plant}}$  enhancements of between 5–80% above ambient. Searles et al.<sup>11</sup> divided their analysis of 103 studies into  $UV_{\text{plant}}$  increases simulating ozone depletions of 10–20% and those to simulating depletions exceeding 20%, broadly equivalent to increases in  $UV_{\text{plant}}$  of 20–40% and exceeding 40%, respectively. However, none of these other meta-analyses quantify the relationship between  $UV_{\text{plant}}$  and the plant response (e.g. by regression). Therefore, we estimated the minimum UV response strength for plants for the different  $UV_{\text{plant}}$  exposure categories. We did this by assuming that the mean plant

response in the high and low  $UV_{\text{plant}}$  categories is indicative of the top end of the  $UV_{\text{plant}}$  range (see the “response strength” columns in Extended Data Table 2). This results in the most conservative estimate of plant response to increased  $UV_{\text{plant}}$ . The resulting range of sensitivities we infer from the meta-analyses informed our sensitivity simulations. Our highest dose response, 4.5% reduction in carbon assimilation for a 10% increase in  $UV_{\text{plant}}$  (1.5x reference strength) is actually conservative compared with some the individual results of specific meta-analysis for particular growth parameters. On the other hand, our lowest sensitivity, 0.3% reduction in biomass for a 10% increase in  $UV_{\text{plant}}$  (0.1x reference strength), is representative of minimum reductions in above ground-biomass across the meta-analyses.

Even with this range of sensitivities, two uncertainties remain. The first is the magnitude of plant responses to the very large ozone depletions that would occur in the second half of the century in the world avoided (Fig. 1d). We recognise that our framework extrapolates data from field experiments into the effects of increased  $UV_{\text{plant}}$  that are generally limited to treatments that simulate up to a two-fold increase (Extended Data Table 2), equivalent to a ~50% depletion of the total ozone column. In qualitative terms, there is support for such extrapolation in the effects of the more severe  $UV_{\text{plant}}$  treatments delivered in controlled environment studies. Such treatments often lead to the significant acute damage of a wide-range of plant processes, and while they have sometimes been described as an ‘unrealistic’ UV environment given current and projected ozone columns, they may illustrate the severe damage that would occur under extreme ozone depletions. That has not been confirmed under field conditions, but we consider much smaller responses through our sensitivity analysis. In particular, our lowest UV response strength (0.1x reference strength) is an order of magnitude less sensitive than our baseline. Overall, we believe that these approaches allow our modelling to illustrate a range of possible outcomes consistent with the uncertainties associated with plant UV dose responses.

The second uncertainty is that almost all experiments into plant responses to UV-B have used the Caldwell action spectrum<sup>36</sup> to calculate  $UV_{\text{plant}}$ , and these form the basis of the meta-analyses that underpin our simulations. Current evidence indicates that assuming an alternative action spectrum (e.g., Flint and Caldwell<sup>52</sup>) either has little effect on the interpretation of experiments designed using Caldwell-weighted  $UV_{\text{plant}}$ <sup>53</sup> or that experiments have under-estimated the increase in UV required to simulate a given ozone depletion<sup>54</sup>.

### **JULES land surface model**

We simulated the land surface with the Joint UK Land Earth Simulator (JULES) model<sup>29,30</sup> version 5.2. Taking meteorological input from the weather generator (precipitation, surface temperature, humidity, pressure, winds and downwelling longwave and shortwave fluxes), JULES calculates momentum, water and heat land-atmosphere exchanges, and additionally  $CO_2$  transfer, by the balance of gross photosynthetic gain and various respiration losses. The vegetation and soil carbon pools were updated on a daily basis, holding the areal fractions of

plant functional types fixed to observed 2010 values to allow for a clean comparison between the simulations. This, and the fact that all plant types have a minimum leaf area index of 1, means that vegetation feedbacks are limited and therefore the impacts on NPP are conservative. Land cover was from the European Space Agency Land Cover Climate Change Initiative<sup>55</sup> translated to nine plant functional types<sup>56</sup> and this version of the model has been shown to realistically capture present-day transient land carbon uptake<sup>57</sup>. The CO<sub>2</sub> exchanges are spatially and temporally integrated to provide estimates of global terrestrial carbon stocks. The land-atmosphere CO<sub>2</sub> exchange is controlled by near-surface meteorology and by atmospheric CO<sub>2</sub> concentrations (appropriate to the RCP6.0 scenario used here), which, all things being equal, increase the rate of carbon uptake (i.e., CO<sub>2</sub> fertilisation)

The additional impact of UV<sub>Plant</sub> was captured by scaling of the net carbon uptake term in JULES with an all-sky UV scale factor (0–1), chosen as an appropriate way to capture the UV impact at this large scale. This scale factor is applied on a daily time step and was derived from a downward adjustment of clear sky UV scale factor due to any clouds, calculated by ratioing the daily totals of the all-sky downwelling surface shortwave radiation (SW) and the clear sky downwelling surface SW from the weather generator. For example, in the base case simulations, if clear sky UV scale factor is 0.95 (5% damage) but cloud cover is 50% all day, all-sky UV scale factor becomes 0.975. Averaged across all land surfaces, and using the reference UV response strength, we see a 1.2% reduction in global mean net primary productivity per 10% increase in the all-sky UV scale factor. The effect is stronger in the northern temperate (30°N–60°N) and boreal (60°N–82.5°N) zones, but weaker in the tropics (30°S–30°N), where NPP is already high so percentage decreases are low.

### **Offline energy balance and carbon cycle model**

The implications of the UV increases on the broader carbon cycle and global mean surface temperature change, due to lower terrestrial productivity and reduced land storage of carbon, were calculated using a simple global “box” model. The model structure includes a fully-coupled description of land, ocean and atmosphere carbon stocks and the related flows. The global energy balance model is identical to a previously published model<sup>58</sup>, although the four parameters for the governing equations are calibrated against the newer HadGEM2-ES Earth system model, from which NIWA-UKCA is closely related. These four parameters are 1) global ocean heat diffusivity, the equilibrium climate sensitivity to increased radiative forcing over 2) land and 3) ocean, and 4) the land-to-ocean surface warming ratio. The radiative forcing for varying atmospheric CO<sub>2</sub> is the standard logarithmic description, as is also used when we model carbon cycle feedbacks (see below). Other radiatively-active gases, where not perturbed by ozone-depleting substances, follow the standard radiative forcing pathways for the appropriate RCP scenarios<sup>59</sup>.

The carbon cycle description consists of prescribed emissions of CO<sub>2</sub>, which add to the atmospheric concentration of that gas, which are then modulated further by exchanges with the land and oceans. Atmosphere-ocean carbon dioxide fluxes are dependent on historical temperature and CO<sub>2</sub> levels<sup>60</sup>. The land-atmosphere CO<sub>2</sub> exchange is also interactive with the atmospheric CO<sub>2</sub> concentrations. The land surface is described using a perturbation approach<sup>61</sup>, with changes to carbon stores increasing linearly in atmospheric CO<sub>2</sub> (CO<sub>2</sub> fertilisation) and decreasing linearly in global warming (enhanced respiration). The linear coefficients are the mean values from across land surface models<sup>56</sup>. The time-evolving JULES model response to UV damage is mapped on to this framework, calculated as a fraction of terrestrial carbon suppression, for the simulations corresponding to the worldAvd and the worldProj scenarios. In our coupled system, the linear perturbation of land stores is added to pre-industrial estimates of the amount of terrestrial carbon. These time-evolving estimates of carbon stores<sup>61</sup> are modified by the JULES-based fractional suppression.

The box model was operated using the identical RCP6.0 forcings used to drive the NIWA-UKCA and JULES simulations. This forcing includes the prescription of atmospheric CO<sub>2</sub> concentrations, and so the box model was initially inverted to generate the associated trajectory of CO<sub>2</sub> emissions (with the UV impact switched off). The model was then operated in forward mode and forced with these calculated emissions, completing runs with the UV-suppression of carbon stocks switched on and off. With the suppression off, the forward projections of temperature and CO<sub>2</sub> were verified as matching those in the inversion simulation. Then, running the box model with the suppression on, and comparing to when off, allowed us to quantify the impact of terrestrial ecosystem UV damage on levels of global warming and the atmospheric CO<sub>2</sub> trajectory, with all carbon cycle feedbacks represented. We quantify these global temperature and CO<sub>2</sub> impacts due to the UV damage for both the worldAvd and worldProj scenarios. Finally, we also note that the additional atmospheric CO<sub>2</sub> in the worldAvd forces a higher land-atmosphere sink, i.e., CO<sub>2</sub> fertilisation. Our presented results include this fertilisation effect, but without it we estimate that the resulting higher atmospheric CO<sub>2</sub> concentrations would have resulted in a temperature increase that is approximately 25% higher than we report.

### **Data availability**

All relevant JULES and NIWA-UKCA model output and input data has been archived as a Zenodo repository, where it has been given the following doi: [10.5281/zenodo.4733883](https://doi.org/10.5281/zenodo.4733883).

### **Code availability**

The JULES code for these simulations is available on the Met Office Science Repository System (MOSRS) (<https://code.metoffice.gov.uk/trac/jules>) (registration required) in revision 15798. Simulations were run using the Rose suite u-bb620, also available through the MOSRS. The NIWA-UKCA CCM is based on the HadGEM3 climate model which is available under licence. Please contact author OM for details.

## References (Methods only)

44. Morgenstern, O. *et al.* Evaluation of the new UKCA climate-composition model—Part 1: The stratosphere. (2009).
45. Hewitt, H. T. *et al.* Design and implementation of the infrastructure of HadGEM3: The next-generation Met Office climate modelling system. *Geoscientific Model Development* **4**, 223–253 (2011).
46. WMO (World Meteorological Organization). *Scientific Assessment of Ozone Depletion: 2010*, Global Ozone Research and Monitoring Project—Report No. 52, Geneva, Switzerland (2011).
47. Morgenstern, O. *et al.* Ozone sensitivity to varying greenhouse gases and ozone-depleting substances in CCM1-1 simulations. *Atmos. Chem. Phys.* **18**, 1091–1114 (2018).
48. Edwards, J. M. & Slingo, A. Studies with a flexible new radiation code. I: Choosing a configuration for a large-scale model. *Quart. J. Roy. Meteor. Soc.* **122**, 689–719 (1996).
49. Forster, P. M. *et al.* Evaluation of radiation scheme performance within chemistry climate models. *J. Geophys. Res.* **116**, D10302 (2011).
50. Lauer, A. & Hamilton, K. Simulating clouds with global climate models: A comparison of CMIP5 results with CMIP3 and satellite data. *J. Clim.* **26**, 3823–3845 (2013).
51. Dee, D. P. *et al.* The ERA-Interim reanalysis: Configuration and performance of the data assimilation system. *Quart. J. Roy. Meteor. Soc.* **137**, 553–597 (2011).
52. Flint, S. D. & Caldwell, M. M. A biological spectral weighting function for ozone depletion research with higher plants. *Physiol. Plant.* **117**, 137–144 (2003).
53. Kotilainen, T., Lindfors, A., Tegelberg, R. & Aphalo, P. J. How realistically does outdoor UV-B supplementation with lamps reflect ozone depletion: An assessment of enhancement errors. *Photochem. Photobiol.* **87**, 174–183 (2010).
54. Flint, S. D., Ryel, R. J. & Caldwell, M. M. Ecosystem UV-B experiments in terrestrial communities: a review of recent findings and methodologies. *Agric. For. Meteorol.* **120**, 177–189 (2003).
55. Poulter, B. *et al.* Plant functional type classification for earth system models: results from the European Space Agency’s Land Cover Climate Change Initiative. *Geoscientific Model Development* **8**, 2315–2328 (2015).
56. Harper, A. B. *et al.* Improved representation of plant functional types and physiology in the Joint UK Land Environment Simulator (JULES v4.2) using plant trait information. *Geoscientific Model Development* **9**, 2415–2440 (2016).
57. Harper, A. B. *et al.* Vegetation distribution and terrestrial carbon cycle in a carbon cycle configuration of JULES4.6 with new plant functional types. *Geoscientific Model Development* **11**, 2857–2873 (2018).
58. Huntingford, C. & Cox, P. M. An analogue model to derive additional climate change scenarios from existing GCM simulations. *Clim. Dyn.* **16**, 575–586 (2000).
59. Meinshausen, M. *et al.* The RCP greenhouse gas concentrations and their extensions from 1765 to 2300. *Clim. Change* **109**, 213–241 (2011).
60. Huntingford, C. *et al.* Using a GCM analogue model to investigate the potential for Amazonian forest dieback. *Theor. Appl. Climatol.* **78**, 177–185 (2004).
61. Friedlingstein, P. *et al.* Climate–carbon cycle feedback analysis: Results from the C4MIP model intercomparison. *J. Clim.* **19**, 3337–3353 (2006).

## **Acknowledgements**

PJY was supported by the UK Engineering and Physical Science Research Council (grant EP/R01860X/1), the Natural Environment Research Council (grant NE/R004927/1) and by the Faculty of Science and Technology at Lancaster University. ABH acknowledges funding from the UK Engineering and Physical Science Research Council (Fellowship EP/N030141/1) and Natural Environment Research Council (grant NE/P019951/1). CH acknowledges the UK National Capability grant given to the UK Centre for Ecology and Hydrology. OM was supported by the NZ Government's Strategic Science Investment Fund (SSIF) through the NIWA programme CACV. LDO is supported by the NASA Modeling, Analysis, and Prediction program. SM and RRG are supported by the National Center for Atmospheric Research, which is a major facility sponsored by the U.S. National Science Foundation under Cooperative Agreement No. 1852977. All authors acknowledge the contribution of New Zealand's national high-performance computing facilities to the results of this research, provided by the NZ eScience Infrastructure (NeSI) and funded jointly by NeSI's collaborator institutions and through the NZ Ministry for Business, Innovation and Employment's Research Infrastructure Programme.

## **Author contributions**

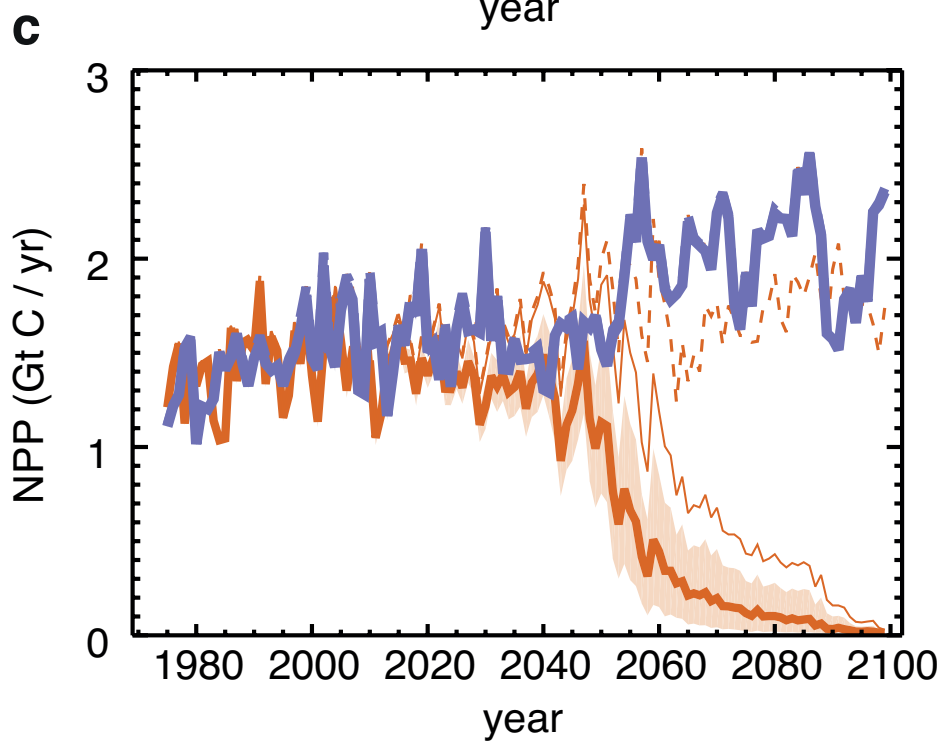
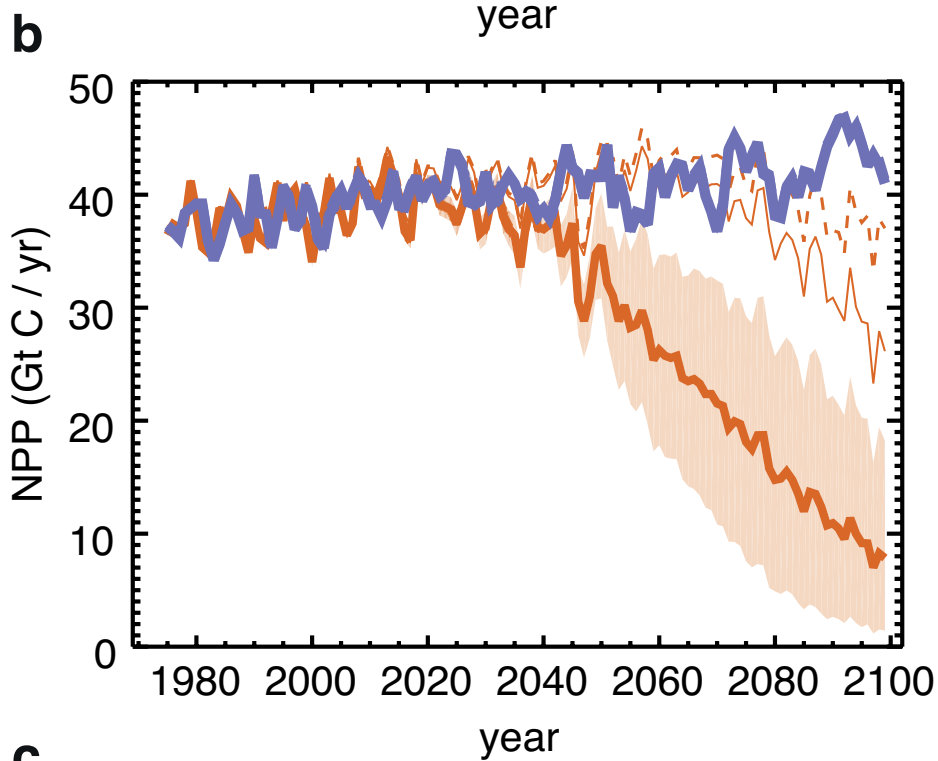
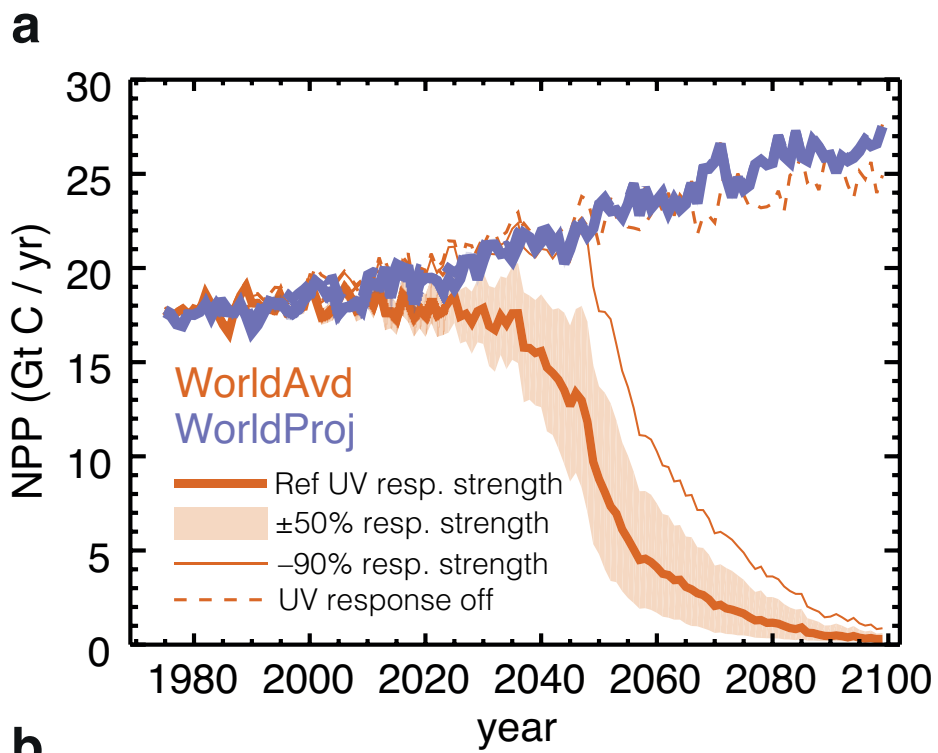
PJY conceived the initial study based on conversations with NDP. PJY, ABH and CH designed and constructed the modelling framework and the simulations, performed the analysis, and wrote the manuscript with NDP. OM, PAN, LDO, SM and RRG provided model simulation data to run the framework, input to the parameterisations used, and contributed to the manuscript writing.

## **Competing interests**

The authors declare no competing interests.

## **Additional information**

Correspondence and requests for materials should be addressed to PJY.



	RCP6.0 (worldAvd)		RCP2.6		RCP8.5	
	vs worldProj	vs UV resp. 0	vs worldProj	vs UV resp. 0	vs worldProj	vs UV resp. 0
$\Delta\text{CO}_2$ / ppm	191 (147–235)		165 (127–203)		216 (165–265)	
$\Delta\text{GSAT}$ / K	2.5 (2.4–2.7)	0.85 (0.65–1.0)	2.7 (2.5–2.9)	1.0 (0.80–1.3)	2.4 (2.3–2.6)	0.74 (0.56–0.90)



## Extended data captions

**Extended data Fig. 1 | Impacts on net primary productivity for different latitude bands.** Net primary productivity (NPP) time series data from JULES, as per Fig. 2a, but for (a) 30°N–60°N, (b) 30°S–30°N and (c) 55°S–30°S.

**Extended data Table 1 | UV impact on CO<sub>2</sub> and global mean air temperature for different scenarios.** The impact of the underlying climate scenario on the end century (2080–2099 average) atmospheric CO<sub>2</sub> concentrations and resulting global mean air temperature (GSAT) change, as calculated using the offline energy balance model and carbon cycle model. Results are included for the worldProj (refC2 = RCP6.0), as reported in the main manuscript, alongside for RCP2.6 and RCP8.5. For each scenario, the left hand column shows the additional CO<sub>2</sub> and temperature change arising in the worldAvd simulations, calculated by comparison against the equivalent worldProj simulation. In addition, the right hand column shows the extra temperature change resulting from including the UV effect in worldAvd (i.e., resulting from the additional atmospheric CO<sub>2</sub> concentrations), calculated by comparison against the worldAvd simulation with the UV response strength set to zero. The central value is for the reference UV response strength and the range is from the ±50% UV response strength sensitivity simulations.

### **Extended Data Table 2 | The plant-UV meta-analyses that informed our simulations.**

Overview of the meta-analyses of plant responses to plant-weighted UV-B radiation ( $UV_{\text{plant}}$ ) that informed the quantitative responses (% change in plant biomass for a 10% increase in  $UV_{\text{plant}}$ ) in the sensitivity analysis of our model. Data are taken from the meta-analyses of Newsham and Robinson<sup>9</sup>, Searles et al.<sup>11</sup>, Li et al.<sup>10</sup> and Fu and Shen<sup>12</sup>, which cover a range of plant types and geographies. The table summarises the  $UV_{\text{plant}}$  exposures (as percentage above ambient) that each of the meta-analyses consider, the mean plant response (across above ground biomass, all biomass and/or leaf area), and the inferred minimum plant response (% response for 10% increase in  $UV_{\text{plant}}$ ) from those ranges, which is calculated from the maximum of the range divided by mean response. The symbols in the table refer to the following notes: (\*) Since Searles et al. divided their meta-analysis in terms of simulated ozone depletions, we estimated the equivalent in terms of increases in  $UV_{\text{plant}}$  using the widely cited value of 2.0 for the radiation amplification factor. (†) Newsham and Robinson included field experiments using filters that reduced  $UV_{\text{plant}}$  below ambient. (‡) The cited means are those cited in each meta-analysis for a given range of increases in  $UV_{\text{plant}}$ . (§) UV response strengths (% change in plant biomass for a 10% increase in  $UV_{\text{plant}}$ ) is calculated assuming that all experiments within a given category used the maximum increase in  $UV_{\text{plant}}$ , resulting in the most conservative estimate of UV response strength. (||) These values are derived from the regressions given by Newsham and Robinson. The plot for above-ground biomass is the basis of the “3% reduction in biomass for a 10% increase in  $UV_{\text{plant}}$ ” proposed by Ballaré et al.<sup>8</sup>, which is a rounded value of the slope of the relationship (–3.2) in our regression analysis of Newsham and Robinson. (¶) Searles et al. cite

these values for two different analyses of the full range of  $UV_{\text{plant}}$  increases (20–100%) in their meta-analysis. (#) Fu & Shen do not separate different ranges of  $UV_{\text{plant}}$  treatments, but their supplementary data indicate that the experiments they analysed used enhancements of between 5% and 80% above ambient.